



## IN SITU MEASUREMENTS OF ATMOSPHERIC CO AND ITS CORRELATION WITH NO<sub>x</sub> AND O<sub>3</sub> AT A RURAL MOUNTAIN SITE

Jingsong Li<sup>1,2</sup>, Andreas Reiffs<sup>1</sup>, Uwe Parchatka<sup>1</sup>, Horst Fischer<sup>1</sup>

1) Max Planck Institute for Chemistry, Hahn-Meitner-Weg 1, 55128 Mainz, Germany (✉horst.fischer@mpic.de)

2) Anhui University, Key Laboratory of Opto-Electronic Information Acquisition and Manipulation of Ministry of Education, Hefei, 230601, China. (ljs0625@126.com)

### Abstract

Ambient concentrations of CO, as well as NO<sub>x</sub> and O<sub>3</sub>, were measured as a part of the PARADE campaign conducted at the Taunus Observatory on the summit of the Kleiner Feldberg between the 8th of August and 9th of September 2011. These measurements were made in an effort to provide insight into the characteristics of the effects of both biogenic and anthropogenic emissions on atmospheric chemistry in the rural south-western German environment. The overall average CO concentration was found to be 100.3±18.1 ppbv (within the range of 71 to 180 ppbv), determined from 10-min averages during the summer season. The background CO concentration was estimated to be ~90 ppbv. CO and NO<sub>x</sub> showed bimodal diurnal variations with peaks in the late morning (10:00-12:00 UTC) and in the late afternoon (17:00-20:00 UTC). Strong correlations between CO and NO<sub>x</sub> indicated that vehicular emission was the major contributor to the notable CO plumes observed at the sampling site. Both local meteorology and backward trajectory analyses suggest that CO plumes were associated with anthropogenically polluted air masses transferred by an advection to the site from densely populated city sites. Furthermore, a good linear correlation of  $R^2 = 0.54$  between CO and O<sub>3</sub> ( $\Delta O_3/\Delta CO = 0.560 \pm 0.016$  ppbv/ppbv) was observed, in good agreement with previous observations.

Keywords: Trace gas measurements, atmospheric CO, QCL sensor, sources relation, sources identification.

© 2015 Polish Academy of Sciences. All rights reserved

### 1. Introduction

Carbon monoxide (CO) is considered to be one of the most important atmospheric trace gases that play a key role in the oxidative chemistry of the troposphere [1–3]. It is an important trace gas for the budget and distribution of the hydroxyl (OH) radical, which exerts a controlling influence on the gas phase chemistry of many atmospheric species. The reaction of OH and CO is believed to be a major mechanism for removal of atmospheric OH. An increase in CO could lead to a corresponding decrease in OH, thereby reducing the ability of the troposphere to scavenge other greenhouse gases such as methane (CH<sub>4</sub>) and other volatile organic compounds (VOCs). CO has a mean atmospheric lifetime of about two months in summer against oxidation by OH. The CO mixing ratio exhibits a highly spatial and temporal variance, and ranges from around tens of ppbv (lower stratosphere) to ~100 ppbv in a clean atmospheric troposphere [4]. The main sources of CO are photo-chemical production from oxidation of methane and non-methane hydrocarbons, biomass burning and incomplete combustion of carbon-based fuels that are widely used for power generation, industrial heating, petrochemical refining, and propulsion [5–7]. Due to its moderately long lifetime, CO is considered as an ideal tracer of atmospheric transport processes, and it is also a useful indicator of the anthropogenic pollution and biomass burning [8].

Measurements of atmospheric CO have been made by many laboratories around the world using a variety of analytical techniques. Most of the techniques used for measuring CO are

described by Novelli [9], including GC-HgO (Gas Chromatography with a mercuric oxide detector), GC-FID (Gas Chromatography with a Flame Ionization Detector), NDIR (Non-Dispersive Infrared Absorption), Gas Filter Correlation, and VUVF (Vacuum Ultra-Violet Fluorescence), as well as a semiconductor gas sensing method [10]. Recently, new spectroscopic techniques such as a CRDS (Cavity Ring-Down Spectroscopy), an ICOS (Integrated Cavity Output Spectroscopy) and a mid-infrared (MIR) direction absorption spectroscopy have been demonstrated for high precision CO measurements in the ambient air, as well as for the calibration of standards [10]. The MIR spectroscopy has proven to be a powerful technique for the atmospheric trace gases detection with a high precision, accuracy, high specificity and fast time resolution from aircraft, balloons, ship-based and mobile van platforms, as well as from fixed sites at remote locations [11–14]. The small size, simplicity, high output power, wide tunable frequency range and long-term reliability of novel quantum cascade lasers (QCLs) are promising MIR spectroscopic sources, and making them suitable for a wide variety of applications to map stratospheric CO distributions [15–17] and to perform isotopic measurements [18–19], high temperature combustion diagnoses [20] and human breath analyses [21].

In the present study, measurements of atmospheric carbon monoxide at a rural site were performed using a novel continuous-wave (CW) room temperature (RT) QCL based sensor during the summer 2011 PARADE field campaign at Taunus Observatory, a low elevation mountain site in south-western Germany. The sampling had been done at a high frequency (1 second) for approximate one month, to provide insights into short-term variability and diurnal cycles. Ancillary measurements of nitrogen oxides (NO and NO<sub>2</sub>), O<sub>3</sub> and meteorological parameters enabled us to study the oxidative chemistry of the troposphere and the air mass origin at the measurement site.

The paper is structured as follows: In Sect. 2, we describe the instrumentation and typical measurement procedure as well as the sampling site. We then present time series of CO mixing ratios and discuss the diurnal variability and correlations with other species (NO<sub>x</sub> and O<sub>3</sub>). Finally, we present a case study of high CO plumes observed at the sampling site and analyse these high plumes by combining local meteorological parameters and regional atmospheric transport model, HYSPLIT (HYbrid Single-Particle Lagrangian Integrated Trajectory).

## 2. Method and instrumentation

### 2.1. CO measurements

The RT-QCL system employed in the field campaign is a new generation instrument developed by our group. It has been designed for real-time monitoring of atmospheric trace gases. Details of the RT-QCL sensor have been described previously [22]. Here, only a brief overview will be presented. The QCL-based sensor uses a wavelength modulation spectroscopy technique (WMS) and consists of a CW- QCL operating in the wavelength region of 4.56 μm (2188 to 2202 cm<sup>-1</sup>), a multi-pass cell and a reference cell, and two room temperature detectors. The laser beam is firstly collimated and sent through an astigmatic Herriott absorption cell of 300 ml (AMAC-36, Aerodyne Research, USA), offering a total optical path length of 36 m and which consists of two concave mirrors where light is reflected multiple times, enhancing the effective path length through the breath sample. After exiting the absorption cell, the QCL beam is re-collimated and divided by a CaF<sub>2</sub> beam splitter into a reference and signal part. The reference beam is sent to a short reference cell (3.5 cm) with low pressure pure CO for laser frequency locking. Finally, both laser beams are focused onto two TE-cooled mercury cadmium telluride detectors (PVI-4TE-5, Vigo System) working at

the room temperature, thus eliminating a need for liquid nitrogen cooling, simplifying daily use of the system and allowing a long-term automated operation.

In order to improve the sensitivity, the WMS is implemented by modulating the injection current of the laser with the combination of a low frequency triangle ramp (30.5 Hz) for wavelength tuning and a high frequency sinusoidal modulation (31.5 kHz). The 2nd harmonic signal of WMS is demodulated at the double modulation frequency using a digital lock-in amplifier programmed with the Labview software. The ambient CO concentration is determined by fitting the ambient spectra to the calibration spectra measured from standard gas cylinders with a known concentration, using a multiple linear regression algorithm [23].

### *Measurement Procedure and Performance*

For the field deployment, the instrument was installed in an air-conditioned mobile laboratory container used previously for various ground- and ship-based field campaigns, together with other instruments (for HCHO, H<sub>2</sub>O<sub>2</sub>, NO/NO<sub>2</sub> and O<sub>3</sub> measurements). For ambient CO measurements, a constant sample flow of 1.21 SLM (standard litres/min) was shared from the main sampling line. The main air inlet (½ inch PTFE tube, about 15 m length) extends through a hole in the roof of the container to sample the ambient air on the upper platform (~ 10 m above the mountain ground) with a ~ 20 SLM flow rate.

The CO absorption line at 2190 cm<sup>-1</sup> was selected for its spectroscopic characteristics with respect to the line strength, freeness of cross sensitivity to water vapor and other atmospheric constituents [24], as well as a coincidence with the emission wavelength of the available QCL. Since the detection technique employs an indirect spectroscopic method, a suitable calibration procedure had to be developed for retrieving the ambient CO concentration. Typically, a 1-hour calibration cycle was used during the entire field campaign. During the initial stage (10 - 22 Aug.), a single measurement cycle consisted of a 1 min working standard (primary standard, 94 ppbv) for acquiring calibration spectra, followed by a periodic measurement of 9-min real ambient air spectra and 1-min reference spectra (commercial compressed air, 269 ppbv) for evaluating the instrument performance (stability and precision) during each calibration cycle (i.e. 1-hourly interval). Considering the gas stabilisation periods (a sampling delay of ~ 3 s) during each gas exchange process, the instrument thus had a duty cycle of ~88.3%. At a later stage (23 Aug. - 09 Sep.), the reference sample was no longer used, thus increasing the duty cycle to ~ 98.3%. Additionally, non-periodic calibrations of the working standard are accomplished by using cylinders of two known air-CO mixtures (Scott Marrin Specialty Gases, Inc., CA), which are traced to the NOAA scale.

A typical measurement procedure at the original 1-s time resolution over a 1-hour calibration cycle is shown in Fig. 1. As can be seen, a replicate precision of 1.04 ppbv ( $\sigma$ , standard deviation) was obtained from 1-min integrations of measurements of a constant reference sample. The measurement precision can be largely improved ( $\sigma_w$ , the standard deviation, as shown in Fig. 1) by using a wavelet filtering technique during post signal processing [25]. With the utilization of wavelet filtering, the instrument performance has been largely improved. Finally, the replicate precision of 1.55 ppbv and 0.79 ppbv (at 269 ppbv, 1 sigma) without and with wavelet filtering, respectively, was obtained during an evaluation cycle of 11 days. The instrument detection limit, based on reproducibility of the zero air measurement, was 3 ppbv for an integration time of approximate 1s. Based on an error propagation analysis of all the random and systematic components, we estimated that ambient CO concentrations were determined with an absolute uncertainty of less than 10%, which is mainly limited by the accuracy of the calibration gas standards.

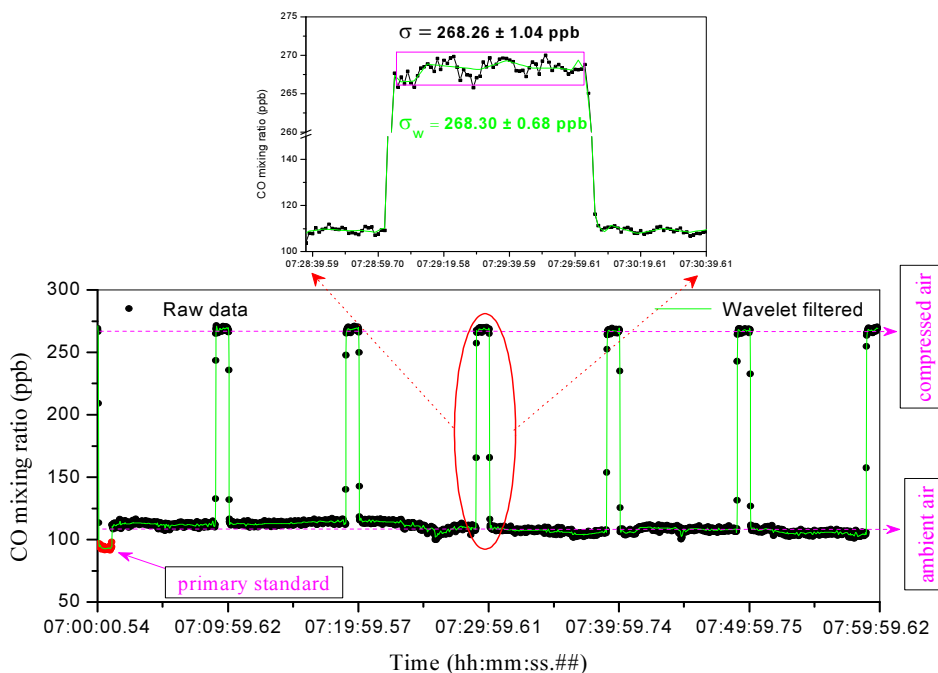


Fig. 1. The lower panel: alternating measurements of a primary standard CO, the compressed air sample from a gas cylinder, and the ambient air during a typical 1-h data acquisition period with the 1 Hz sampling rate. Also shown is the application of a wavelet filter. The upper panel presents a zoom-in on an approximate 2-min measurement interval to indicate the approximate 1-min replicate precision evaluated from the compressed air.

### Site Description

The field deployment of the instrument as a part of the PARADE (PARTICLES and RADICALS: Diel observations of the impact of urban and biogenic Emissions) campaign was conducted at the Taunus Observatory, located at 50°13'25" N, 8°26'56" E and 825 m above the sea level at the summit of the "Kleiner Feldberg", a mountain in the Taunus range in south-western Germany [26]. The area directly around the observatory is mainly covered by the spruce coniferous forest. The hill top itself (50 m in radius) has been cleared of trees for meteorological measurements. The direct vicinity of the measurement containers is covered by shrubs and blueberry plants, except small pine and beech trees at lower levels. The station is known for its quite remote character for central Germany, with only a few main roads and some small towns located within a 5 km area. The PARADE field campaign was undertaken between the 8<sup>th</sup> of August and 9<sup>th</sup> of September 2011. Intensive instruments based on different techniques (optical and non-optical) allow us to examine the effects of both biogenic and anthropogenic emissions on radical chemistry (both day and night). Basic meteorological parameters (e.g. the temperature, pressure, relative humidity, wind speed and wind direction) are measured routinely by the German Weather Service (DWD) station and the local environmental agency station (HLUG) which is located directly next to the measurement site.

### 2.2 NO<sub>x</sub> and O<sub>3</sub> measurements

Collocated with the RT-QCLS in the container was a modified commercial Chemiluminescence Detector (CLD 790 SR) originally manufactured by ECO Physics (Duernten, Switzerland) and a primary standard UV photometric O<sub>3</sub> analyzer (Model 49, Thermo Environmental Instruments Inc.). The two-channel CLD based on the chemiluminescence of the reaction between NO and O<sub>3</sub> was used for measurements of NO and NO<sub>2</sub>. NO<sub>2</sub> was measured as NO using a blue light converter from Droplet Measurement

Technologies, Boulder USA. In the current study, data were obtained at a time resolution of 2 seconds. The CLD detection limits (determined by continuously measuring the zero air at the measuring site) for NO and NO<sub>2</sub> measurements were 4 pptv and 55 pptv, respectively, for an integration period of 2 s. O<sub>3</sub> was measured by UV absorption with a detection limit of 1 ppbv for an integration period of 20 s. The total uncertainties (2σ) for the measurements of NO, NO<sub>2</sub> and O<sub>3</sub> were determined to be 4%, 10% and 5%, respectively, based on the reproducibility of in-field background measurements, calibrations, the uncertainties of the standards and the conversion efficiency of the photolytic converter. For a more detailed discussion of this technique the reader is directed to references [27].

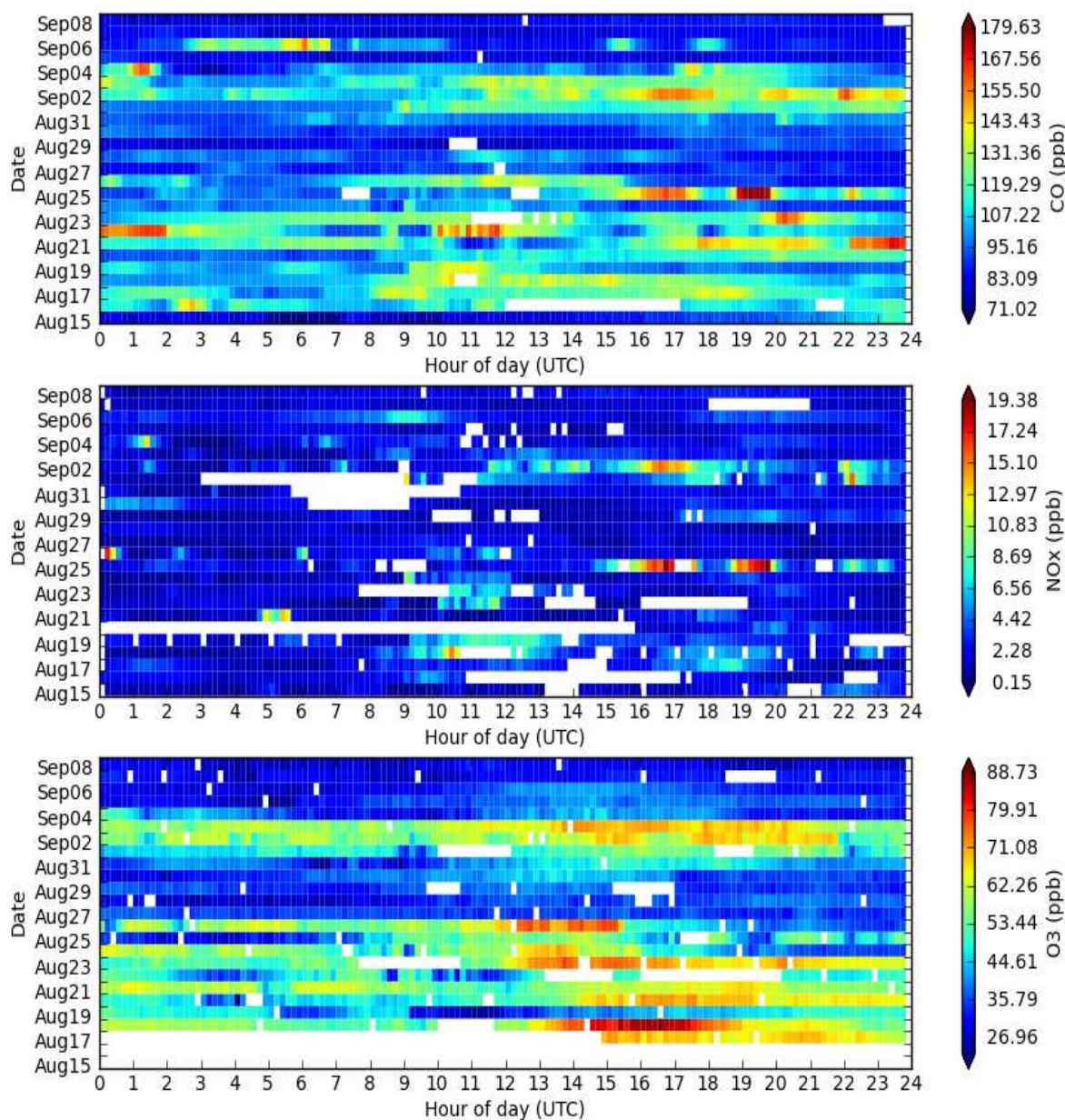


Fig. 2. CO, NO<sub>x</sub> and O<sub>3</sub> variations (the 10-min average interval) over the entire field campaign at Taunus Observatory (UTC = local time – 2 h).

### 3. Results and discussion

#### 3.1. Diurnal variation of CO concentrations

The measurements of ambient CO concentrations were performed originally at a resolution of 1-s. For the inclusion into a merged file containing all data, 10-min averages are calculated and used for this study. Missing data or data gaps are mainly due to the routine calibrations. The data were analysed to examine the diurnal variation of CO in this rural area. The time series (UTC = local time – 2 hours) in Fig. 2, indicates variations of the measured CO from the minimum of 71.0 ppbv to the maximum of 179.6 ppbv (on average,  $100 \pm 18$  ppbv). Most enhancements of CO levels occurred during the afternoon and night hours, except on Sep. 6 when a high CO peak occurred at  $\sim 6:00$  UTC. No regular diurnal pattern with recurring peaks (over 150 ppbv) at fixed hours of the day was observed, indicating that pollution transport to the measurement site was spatially and temporally varying. For NO<sub>x</sub> and O<sub>3</sub>, the observed values are ranging from 0.15 to 19.4 ppbv and from 27 to 88.7 ppbv, respectively.

For a more clear comparison, Fig. 2 (the upper panel) shows the diurnal profiles of 1-hourly average CO and other trace gases (NO<sub>x</sub> and O<sub>3</sub>) mixing ratios during the sampling period. As seen from this figure, the CO concentration retains an almost constant low level (slightly below 100 ppbv) from late midnight (2:00 UTC) to early morning hours (8:00 UTC); this probably indicates the background level of CO at the measurement site. Then, it begins to slowly rise and finally yielding two broadly spread CO plumes in the late morning (9:00–12:00 UTC) and in the late afternoon (16:00–20:00 UTC), respectively. Unlike city areas, the first high CO plume is not observed during the morning rush hours (local time), but several hours later. The second enhancement in CO mixing ratios can be observed with increasing traffic volumes between 15:00–17:00 UTC, followed by a decrease at night due to less CO sources. These broad CO plumes between 9:00–20:00 UTC are potentially due to transport of anthropogenically polluted air mass to the site, rather than being induced by local vehicular emissions.

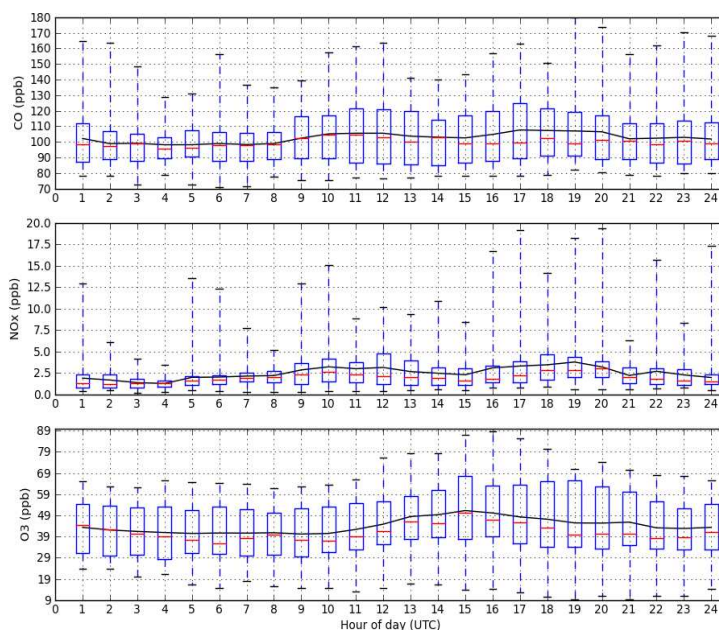


Fig. 3. The diurnal profiles of 1-hourly average trace gases mixing ratios over the entire field campaign at Taunus Observatory. The bottom whisker, box bottom, line inside the box, box top, and top whisker represent the minimum, 25th, 50th, 75th, and maximum of the data, and the continuous lines represent mean values, respectively.

Fig. 3 (middle panel) shows the diurnal profile of  $\text{NO}_x$  mixing ratios at the measurement site that exhibit trends similar to that for CO, with an intermittent increase in the early morning hours (4:00-9:00 UTC), but showing a significant decrease during the night hours (22:00-4:00 UTC). Since both  $\text{NO}_x$  and CO have anthropogenic sources, one would expect these two species to be well correlated if motor vehicle exhaust emissions are important. However,  $\text{NO}_x$  - like CO - peaks occur later than expected morning rush hours showing that emissions take place elsewhere and are subsequently transported to the site. According to the report by Hastie et al.,  $\text{SO}_2$  data can be used to distinguish between  $\text{NO}_x$  and CO from mobile sources and those from stationary sources, as the latter have much higher  $\text{SO}_2$  to  $\text{NO}_x$  ratios [28]. Therefore, by comparison with  $\text{SO}_2$  data measured by another PARADE team, the lack of correlation between  $\text{NO}_x$  (or CO) and  $\text{SO}_2$  (not shown in this study) indicated that the CO and  $\text{NO}_x$  appear to be from mobile sources rather than stationary sources. Since the average wind speed was 3.8 m/s (i.e. 13.8 km/h), and the lifetime of  $\text{NO}_x$  being only a few hours in the planetary boundary layer (PBL) [29], the observed  $\text{NO}_x$  and CO peaks at the measurement site were, on average, produced within a distance of  $\sim 40$  km, assuming that the 3 hours difference from the regular rush hour is the transport time. The  $\text{O}_3$  concentration (Fig. 3, the bottom panel) displayed a typical diurnal variation with the maximum concentration occurring in the afternoon (15:00 UTC), whereas the minimum one - in the early morning (6:00 UTC). The increase and decrease in the  $\text{O}_3$  concentration coincide well with the decrease and increase in the  $\text{NO}_x$  concentration, respectively. The decrease in  $\text{O}_3$  in the night time probably is the result of the dry deposition under the subsiding boundary layer and titration with NO [30].

It is noteworthy that large weekday-weekend differences in CO mixing ratios were observed throughout the measurements (as shown in Fig. 4). The CO build-ups during night hours between 15:00 and 22:00 UTC were higher on weekends than weekdays. This may be attributed to vehicular emissions related to some late night human activities in the warm season. Being a clean rural mountain site, with a limited traffic and no local industries, the strong correlation between CO and  $\text{NO}_x$  indicates that the major pollution sources at the site were vehicular emissions, transferred by an advection to the site from up-wind motorways. This point will be discussed in more detail below.

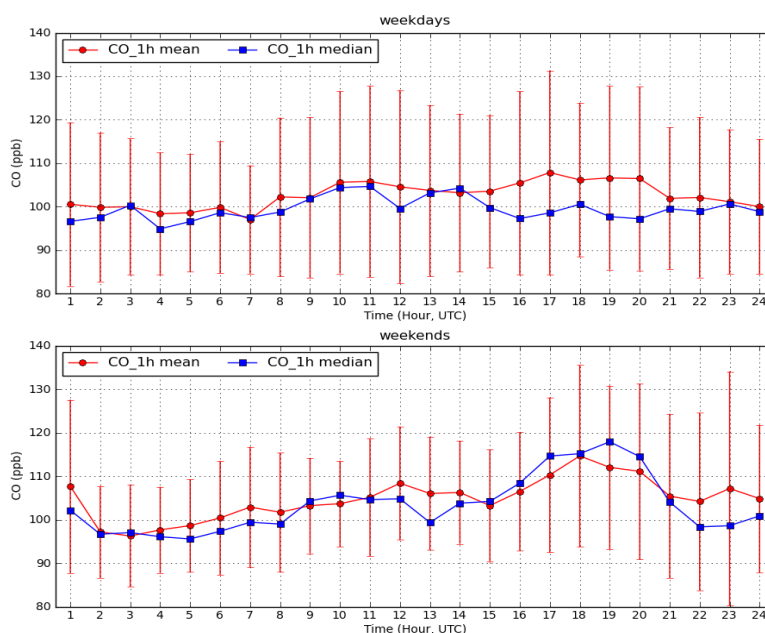


Fig. 4. The diurnal profiles of 1-hourly average CO mixing ratios on weekdays and weekends, respectively.

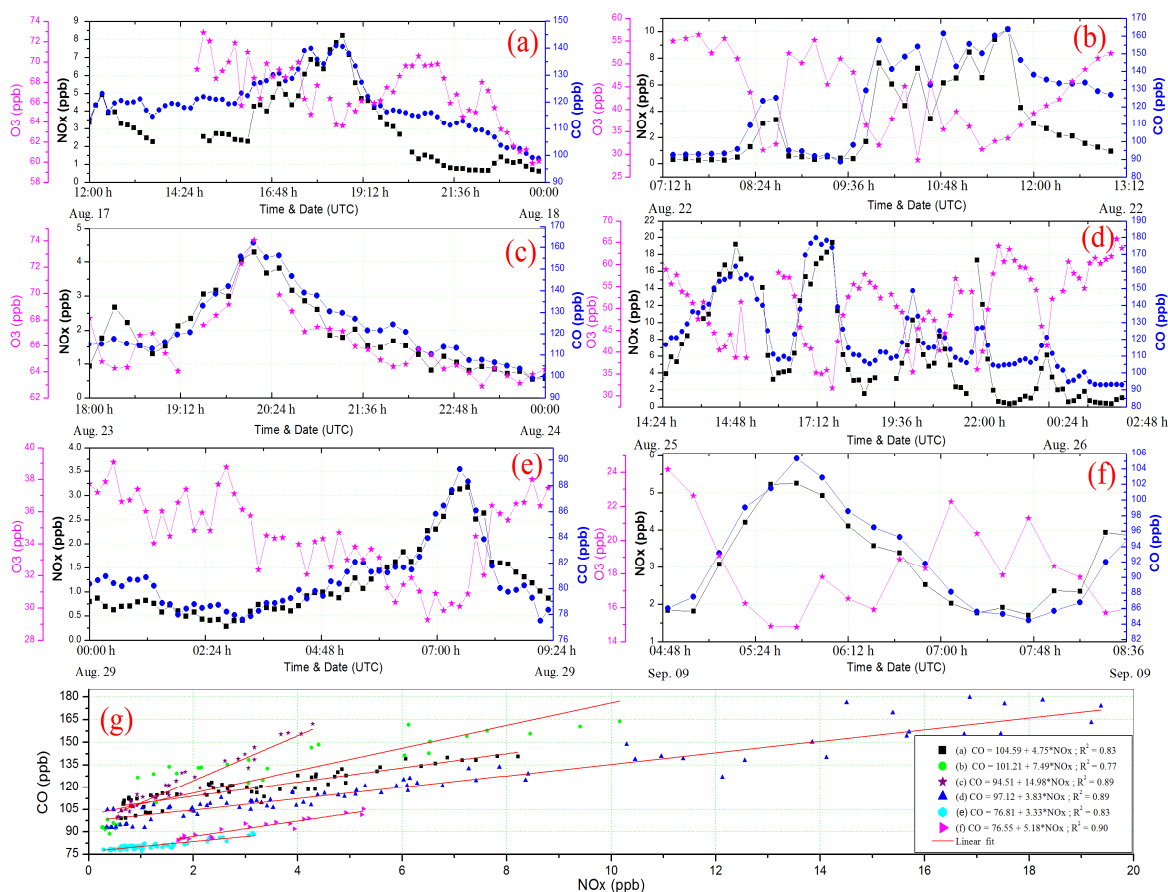


Fig. 5. Time series plots of CO, NO<sub>x</sub> and O<sub>3</sub> for some typical plumes observed over the measurement period (panel a-f), and scatter plots of CO versus NO<sub>x</sub> (panel g). Linear regression fitting parameters are listed in the box.

### 3.2. Correlation between CO and NO<sub>x</sub>

CO is widely considered as a tracer for the anthropogenically polluted air. Similar to NO<sub>x</sub>, it mostly stems from automotive sources in the Rhine-Main area. Thus, it is of interest to investigate the relationship between both species. NO<sub>x</sub> is a generic term for mono-nitrogen oxides, i.e. the sum of NO (nitric oxide) and NO<sub>2</sub> (nitrogen dioxide). In order to assign CO emissions to motor vehicle exhaust sources, we investigate the correlation between CO and NO<sub>x</sub>. For this purpose, we have done a regression analysis for the whole data set from the entire field study. The analysis yielded a poor R<sup>2</sup> of 0.315 and the following dependence:  $[CO] = 4.96(\pm 0.13) \times [NO_x] + 90.26(\pm 0.41)$  ppbv. This relationship suggests that for this rural site in summer time, assuming NO<sub>x</sub> concentrations are near zero, the CO background is approximately 90 ppbv. Two reasons might play a role in the poor correlation. First, the correlation strongly depends on the plume age. Secondly, the emission ratio  $[CO]/[NO_x]$  varies with vehicle types, as is evident in the analysis of individual observed plumes shown in Fig. 5, where the linear regression of 6 typical plumes sampled over the measurement period indicates that the  $[CO]/[NO_x]$  ratio ranges from 3.33 to 14.98 ppbv/ppbv, which is consistent with emission ratios measured by Backer et al. in Germany [31], who reported  $[CO]/[NO_x]$  ratios between 0.63 and 38.33 for vehicles with different fuel types, and mean values of 3.05 and 5.56 for cars and trucks, respectively. Evidently, each plume shows a very high correlation between CO and NO<sub>x</sub> concentrations with R<sup>2</sup> ranging from 0.77 to 0.90. The observed difference in the emission ratios for an individual plume is probably associated with many factors such as an engine/catalyst age and type, an engine state (hot or cold), a fuel type,

a plume age and environment conditions. For example, industry and electrical power generation sources emit little CO; lawn and garden gasoline engines dominate CO emissions, while diesel engines dominate NO<sub>x</sub> emissions; thus, these emission sources will introduce a poor or no-correlation. Generally, the tight correlation between CO and NO<sub>x</sub> concentrations indicate that, despite a clearer environment, these highly correlated plumes observed at the measurement site are potentially due to nearby common sources, or the transport of the polluted air from anthropogenic sources, e.g. the influence of pollution plumes from the Frankfurt city and the Rhine-Main area (such as Mainz and Wiesbaden cities). By referring to the meteorological data and O<sub>3</sub> concentrations, we found that the plume with the highest emission ratio of 14.98 (Fig. 5(c)) was due to the vehicular emissions (relatively fresh air masses) transferred by an advection to the site from up-wind motorways, as mentioned before. Other plumes mainly attributed to the influence of aged air masses from the Frankfurt city (Fig. 5(a) and (d)) and the Rhine-Main area (Fig. 5(b), (e) and (f)). From the point of view of emission ratios, it is difficult to define the difference of air masses from these two locations. However, the results indicate that air masses from the Frankfurt region were normally observed at afternoon and midnight, while those from the Rhine-Main area were observed at morning hours at the sampling site.

### 3.3 Correlation between CO and O<sub>3</sub>

The relationship between O<sub>3</sub> and CO can be used to determine the potential for oxidant that is produced as a result of anthropogenic precursor emissions, and also can be used to distinguish between the fresh emission and the aged air mass. Therefore, we analyzed the whole O<sub>3</sub> and CO dataset using the linear regression, which yielded a slope  $\Delta O_3/\Delta CO$  of  $0.438 \pm 0.011$  ppbv/ppbv, with the correlation coefficient  $R^2$  of 0.33. Generally, when ozone and CO are highly positively correlated, we can conclude that there is a greater oxidant production with increasing the CO concentration, while a highly negative correlation of fresh emissions leads to the titration of O<sub>3</sub> by NO. In the current study, both positive and negative correlations were observed, as shown in Fig. 5. By grouping the data according to the correlation (negative, positive and non-related), an improved positive correlation  $R^2 = 0.54$  with  $\Delta O_3/\Delta CO = 0.560 \pm 0.0156$  ppbv/ppbv can be calculated, which is slightly higher than other measurements (the order of 0.3 ppbv/ppbv) at Izaña observatory, Tenerife, by Fischer et al. [32] and in eastern North American by Parrish et al. [33] and by Chin et al. [34], but consistent with observations ranging from 0.17-0.62 and 0.20-0.69 reported by Wofsy et al. [35] and by Mauzerall et al. [36] observed at surface sites in eastern North America, respectively, as well as 0.4 to 1.0 observed over the eastern United States by Zhang et al. [37]. The negative correlation observed during the night hours for CO values over 100 ppbv might indicate a downward transport of the polluted air to the measurement site after photochemical processing or the O<sub>3</sub> titration by the NO, associated with the freshly emitted CO.

### 3.4 Source identification

In order to investigate the influence of local vs. regional sources on atmospheric CO levels at the measurement site, Fig.6 illustrates the dependence of trace gases (CO, NO<sub>x</sub> and O<sub>3</sub>) and wind speed (WS) mixing ratios on the wind direction (WD) for the duration of the campaign. As expected, the wind rose plot shows that most of high CO levels (over 94.1 ppbv) and other enhanced trace gases (NO<sub>x</sub> and O<sub>3</sub>) were associated with the wind blowing between W-S-W and E-S-E direction where numerous cities (such as Frankfurt, Wiesbaden and Mainz) are located, while the lowest pollution sources are mainly from the directions between W-S-W

and N-N-W, where a broad forest was densely located, but sometimes CO plumes with high concentrations are also observed from these directions, e.g. the CO plume from N-W, which is potentially due to the influence of a motorway located there. In particular, the highest CO levels from S-S-E are closely correlated with the highest NOx levels indicating the influence of the pollution air mass from the Frankfurt city.

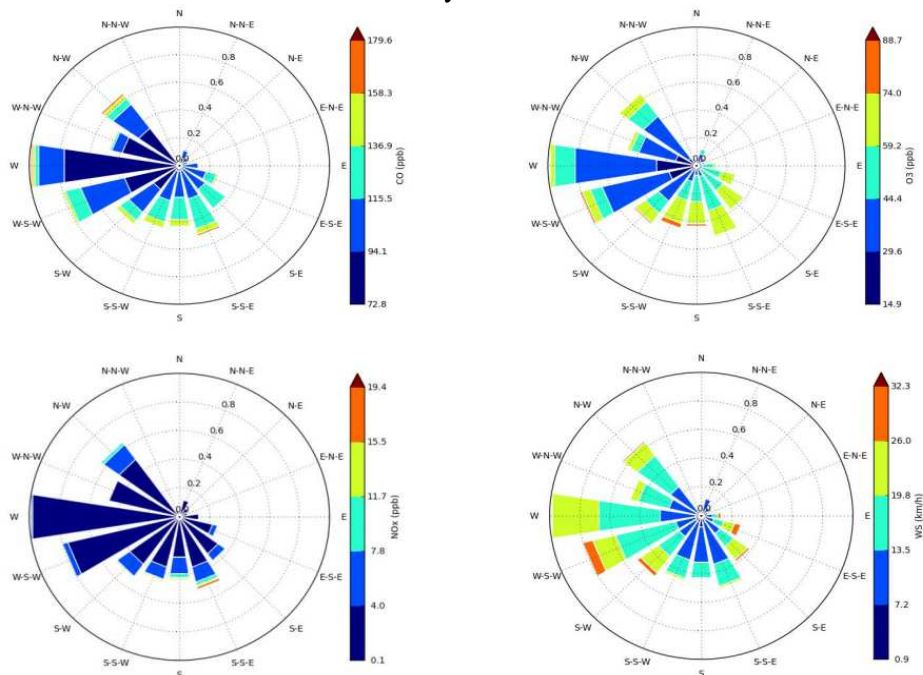


Fig. 6. Wind rose plots showing the dependence of trace gases mixing ratios and the wind speed on the wind direction.

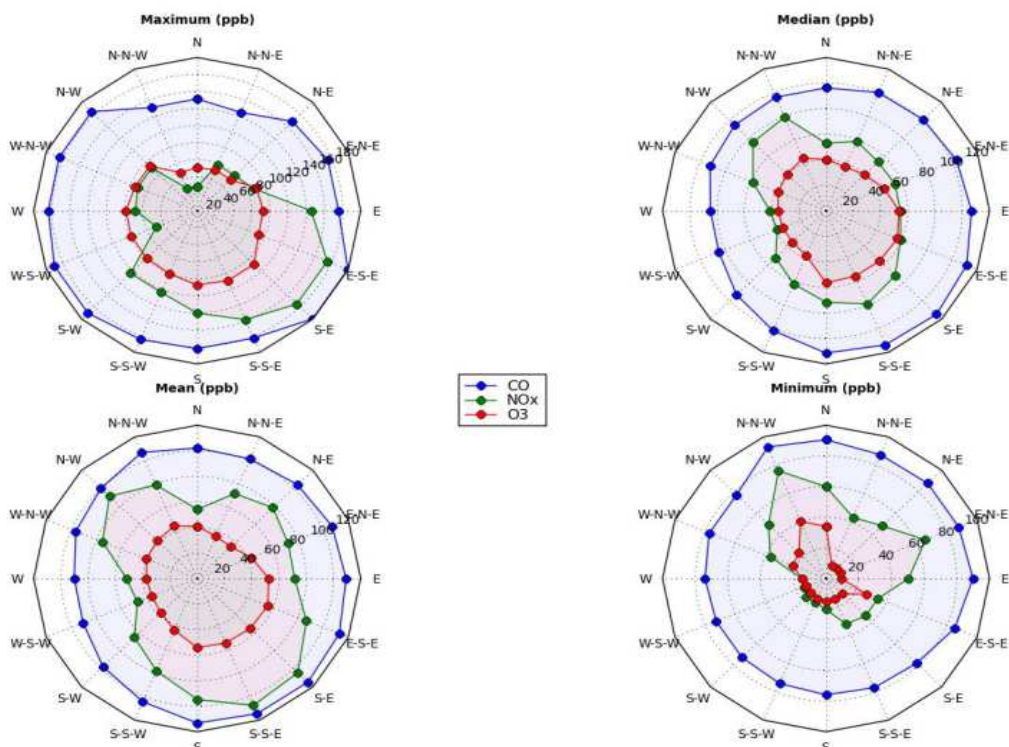


Fig. 7. Wind rose plots showing the statistical results for each trace gas mixing ratio on the wind direction. For clarity, the mean, median, maximum and minimum of NOx data was multiplied by 30, 30, 8 and 100, respectively.

Fig. 7 displays the statistical results for each trace gas mixing ratio on the wind direction. The statistical distributions of CO and NO<sub>x</sub> are quite similar. The maxima and maximum mean and median values for each species are mainly associated with three sectors: S-S-E, S-E and E-S-E (i.e. the direction to the Frankfurt city). The minima and minimum mean and median values also show some distinct dependencies on the wind direction (i.e. between S-W and W-N-W, the direction to the dense broad forest).

The findings mentioned above suggest that the measurement site is significantly influenced by anthropogenically polluted air masses via the atmospheric transport process. Indeed, the influence of pollution plumes from Frankfurt and the Rhine-Main area on the atmospheric component and chemistry of the planetary boundary layer at the Taunus Observatory was also observed by other studies [38].

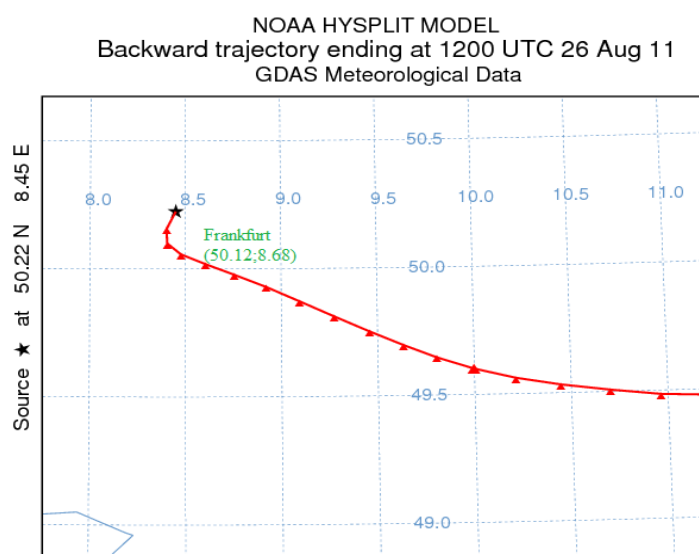


Fig. 8. The backward trajectory calculated by the HYSPLIT model (each triangle represents a 1 h period).

To study the effects of the wind driven long range transport in altering the atmospheric CO level at the measurement site, backward trajectories of 24 hours duration were computed using the NOAA HYSPLIT model available online at [www.arl.noaa.gov/ready/hysplit4.html](http://www.arl.noaa.gov/ready/hysplit4.html). Backward trajectories give only a highly averaged picture, as the minimum data interval available is one hour. Wind trajectories were calculated at the height of 825 m above the mean sea level. As an example, a backward trajectory (see Fig. 8) calculated during 24 hours between 12:00 UTC of Aug. 25 and 12:00 UTC of Aug. 26 depicted a consistent flow of air masses from the Frankfurt city for the high CO plumes shown in Fig. 5(d). Additional analyses suggest that the atmospheric transport from heavily populated cities (e.g. Frankfurt am Main and the Rhine-Main area) by a meteorological situation is a crucial factor in affecting the ambient CO levels of this rural area throughout the whole campaign.

#### 4. Conclusions

In this work we demonstrated in situ atmospheric CO measurement results using a novel RT-QCL based sensor employing high-sensitivity WMS technique with high temporal response. The results showed apparent diurnal variations. Strong correlations between CO and NO<sub>x</sub> indicate the vehicular emissions as the major contributors to the notable CO plumes observed at the sampling site. A combination of a local meteorological situation and backward trajectories analyses suggested that the high CO plumes were associated with anthropogenically polluted air masses by the atmospheric transport from nearby cities, such as

Frankfurt and the Rhine-Main area. We also characterized the oxidant production of ozone, which is consistent with other observations. In the future, other trace gases data will be used to better characterize the importance of CO for the composition and chemistry of the planetary boundary layer and the free troposphere.

### Acknowledgements

The authors would like to thank all the PARADE teams for their hard work, cooperation and enthusiasm in making the PARADE campaign a success. Special thanks go to John Crowley for organizing this field campaign. This work was partly supported by Anhui university personnel recruiting project of academic and technical leaders (Grant No. 10117700014).

### References

- [1] Chameides, W., Walker, J. C. (1973). A photochemical theory of tropospheric ozone. *J. Geophys. Res.-Atmos.*, 78, 8751–8760.
- [2] Logan, J. A., Prather, M. J., Wofsy, S. C., Mcelroy, M. B. (1981). Tropospheric chemistry - a global perspective. *J. Geophys. Res.-Oceans*, 86, 7210–7254.
- [3] Thompson, A. M. (1992). The oxidizing capacity of the earth's atmosphere: probable past and future changes. *Science*, 256, 1157–1165.
- [4] Novelli, P. C., Steele, L. P., Tans, P. P. (1992). Mixing ratios of carbon monoxide in the troposphere. *J. Geophys. Res.-Atmos.*, 97, 20731–20750.
- [5] Graedel T. E., McRae J. E. (1980). On the possible increase of the atmospheric methane and carbon monoxide concentrations during the last decade. *Geophys. Res. Lett.*, 7, 977–979.
- [6] Thompson A. M., Cicerone, R. J. (1986). Possible perturbations to atmospheric CO, CH<sub>4</sub>, and OH. *J. Geophys. Res. - Atmos.*, 91, 10853–10864.
- [7] Wofsy, S. C. (1976). Interactions of CH<sub>4</sub> and CO in the Earth's atmosphere. *Annu. Rev. Earth Pl. Sci.*, 4, 441–469.
- [8] Sze, N. D. (1977). Anthropogenic CO emissions: Implications for the atmospheric CO-OH-CH<sub>4</sub> cycle. *Science*, 195, 673–675.
- [9] Novelli, P. C. (1999). CO in the atmosphere: measurement techniques and related issues. *Chemosphere: Global Change Sci.*, 1, 115–126.
- [10] Heszler, P., Ionescu, R., Llobet, E., Reyes, L. F., Smulko, J. M., Kish, L. B., and Granqvist, C. G. (2007). On the selectivity of nanostructured semiconductor gas sensors. *Physica Status Solidi (b)*, 244, 4331–4335.
- [11] Zellweger, C., Steinbacher, M., Buchmann, B., (2012) Evaluation of new laser spectrometer techniques for in-situ carbon monoxide measurements, *Atmos. Meas. Tech.*, 5, 2555–2567.
- [12] Fried, A., Diskin, G., Weibring, P., Richter, D., Walega, J.G., Sachse, G., Slate, T., Rana, M., Podolske, J. (2008). Tunable infrared laser instruments for airborne atmospheric studies. *Appl. Phys. B* 92, 409–417.
- [13] Wienhold, F. G., Fischer, H., Hoor, P., Wagner, V., Königstedt, R., Harris, G. W., Anders, J., Grisar, R., Knothe, M., W. Riedel, J., Lübken, F.-J., Schilling, T. (1998). TRISTAR—a tracer in situ TDLAS for atmospheric research. *Appl. Phys. B*, 67, 411–417.
- [14] Williams, J., Fischer, H., Hoor, P., Pöschl, U., Crutzen, P.J., Andreae, M.O., Lelieveld, J. (2001). The influence of the tropical rainforest on atmospheric CO and CO<sub>2</sub> as measured by aircraft over Surinam, South America. *Chemosphere: Global Change Sci.*, 3, 157–170.

- [15] Provencal, R., Gupta, M., Owano, T. G., Baer, D. S., Ricci, K. N., O’Keefe, A., Podolske, J. R. (2005). Cavity-enhanced quantum-cascade laser-based instrument for carbon monoxide measurements. *Appl. Opt.*, 44, 6712–6717.
- [16] Schiller, C. L., Bozem, H., Gurk, C., Parchatka, U., Königstedt, R., Harris, G. W., Lelieveld, J., Fischer, H. (2008). Applications of quantum cascade lasers for sensitive trace gas measurements of CO, CH<sub>4</sub>, N<sub>2</sub>O and HCHO. *Appl. Phys. B*, 92, 419–430.
- [17] Viciani, S., D’amato, F., Mazzinghi, P., Castagnoli, F., Toci, G., Werle, P. (2008). A cryogenically operated laser diode spectrometer for airborne measurement of stratospheric trace gases. *Appl. Phys. B*, 90, 581–592.
- [18] Weidmann, D., Wysocki, G., Oppenheimer, C., Tittel, F. K. (2004). Development of a compact quantum cascade laser spectrometer for field measurements of CO<sub>2</sub> isotopes. *Appl. Phys. B*, 80, 255–260.
- [19] Wada, R., Pearce, J. K., Nakayama, T., Matsumi, Y., Hiyama, T., Inoue, G., Shibata, T. (2011). Observation of carbon and oxygen isotopic compositions of CO<sub>2</sub> at an urban site in Nagoya using Mid-IR laser absorption spectroscopy. *Atmos. Environ.*, 45, 1168–1174.
- [20] Vanderover, J., Oehlschlaeger, M. A. (2010). A mid-infrared scanned-wavelength laser absorption sensor for carbon monoxide and temperature measurements from 900 to 4000 K. *Appl. Phys. B*, 99, 353–362.
- [21] Moeskops, B. W. M., Naus, H., Cristescu, S. M., Harren, F. J. M. (2006). Quantum cascade laser-based carbon monoxide detection on a second time scale from human breath. *Appl. Phys. B*, 82, 649–654.
- [22] Li, J. S., Parchatka, U., Königstedt, R., Fischer, H. (2012). Real-time measurements of atmospheric CO using a continuous-wave room temperature quantum cascade laser based spectrometer. *Opt. Express*, 20, 7590–7601.
- [23] Werle, P., Mazzinghi, P., D’Amato, F., De Rosa, M., Maurer, K., Slemr, F. (2004). Signal processing and calibration procedures for in situ diode-laser absorption spectroscopy. *Spectrochim. Acta Part A*, 60, 1685–1705.
- [24] Rothman, L. S., Gordon, I. E., Barbe, A., Benner, D. C., Bernath, P. F., Birk, M., Boudon, V., Brown, L. R., Campargue, A., Champion, J. P. (2009). The HITRAN 2008 molecular spectroscopic database. *J Quant. Spectrosc. Radiat. Transfer*, 110, 533–572.
- [25] Li, J. S., Parchatka, U., Fischer, H. (2012). Applications of wavelet transform to quantum cascade laser spectrometer for atmospheric trace gas measurements. *Appl. Phys. B*, 108, 951–963.
- [26] Crowley, J. N., Schuster, G., Pouvesle, N., Parchatka, U., Fischer, H., Bonn, B., Bingemer, H., Lelieveld, J. (2010). Nocturnal nitrogen oxides at a rural mountain-site in south-western Germany. *Atmos. Chem. Phys.*, 10, 2795–2812.
- [27] Hosaynali Beygi, Z., Fischer, H., Harder, H. D., Martinez, M., Sander, R., Williams, J., Brookes, D. M., Monks, P. S., Lelieveld, J. (2011). Oxidation photochemistry in the Southern Atlantic boundary layer: unexpected deviations of photochemical steady state. *Atmos. Chem. Phys.*, 11, 8497–8513.
- [28] Hastie, D. R., Shepson, P. B., Reid, N., Roussel, P. B., Melo, O. T. (1996). Summertime NO<sub>x</sub>, NO<sub>y</sub>, and ozone at a site in rural Ontario. *Atmos. Environ.*, 30, 2157–2165.
- [29] Browne, E. C., Cohen, R. C. (2012). Effects of biogenic nitrate chemistry on the NO<sub>x</sub> lifetime in remote continental regions. *Atmos. Chem. Phys.*, 12, 11917–11932.
- [30] Aneja, D.S. Kim, W.L. (1997). Chameides, Trends and analysis of ambient NO, NO<sub>y</sub>, CO, and Ozone concentrations in Raleigh, North Carolina. *Chemosphere*, 34, 611–623.
- [31] Becker, K. H., Lörzer, J. C., Kurtenbach, R., Wiesen, P., Jensen, T. E., Wallington, T. J. (1999). Nitrous Oxide (N<sub>2</sub>O) Emissions from Vehicles. *Environ. Sci. Technol.*, 33, 4134–4139.
- [32] Fischer, H., Nikitas, C., Parchatka, U., Zenker, T., Harris, G. W., Matuska, P., Schmitt, R., Mihelcic, D., Muesgen, P., Paetz, H.-W., Schultz, M., Volz-Thomas, A. (1998). Trace gas measurements during the Oxidizing Capacity of the Tropospheric Atmosphere campaign 1993 at Izaña. *J. Geophys. Res.-Atmos.*, 103, 13505–13518.

- [33] Parrish, D. D., Buhr, M. P., Trainer, M., Norton, R. B., Shimshock, J. P., Fehsenfeld, F. C., Anlauf, K. G., Bottenheim, J. W., Tang, Y. Z., Wiebe, H. A., Roberts, J. M., Tanner, R. L., Newman, L., Bowersox, V. C., Olszyna, K. J., Bailey, E. M., Rodgers, M. O., Wang, T., Berresheim, H., Roychowdhury, U. K., Demerjian, K. L. (1993). The total reactive nitrogen levels and the partitioning between the individual species at six rural sites in eastern North America. *J. Geophys. Res.-Atmos.*, 98, 2927–2939.
- [34] Chin, M., Jacob, D. J., Munger, J. W., Parrish, D. D., Doddridge, B. G. (1994). Relationship of ozone and carbon monoxide over North America. *J. Geophys. Res.-Atmos.*, 99, 14565–14573.
- [35] Wofsy, S. C., Sachse, G. W., Gregory, G. L., Blake, D. R., Bradshaw, J. D., Sandholm, S. T., Singh, H. B., Barrick, J. A., Harriss, R. C., Talbot, R. W. (1992). Atmospheric Chemistry in the Arctic and Subarctic: Influence of Natural Fires, Industrial Emissions, and Stratospheric Inputs, *J. Geophys. Res. - Atmos.*, 97, 16731–16746.
- [36] Mauzerall, D. L., Jacob, D. J., Fan, S. -M., Bradshaw, J. D., Sandholm, S. T., Blake, D. R., Gregory, G. L., Sachse, G. W. (1993). An ozone budget for the remote troposphere over eastern Canada. *Eos Trans. AGU*, 74, *Fall Meeting Supplement* 74,180. San Francisco, USA.
- [37] Zhang, L., Jacob D., Bowman, K., Logan, J. A., Turquety, S., Hudman, R. C., Li, Q., Beer, R., Worden, H., Worden, J., Rinsland, C. P., Kulawik, S. S., Lampel, M. C., Shephard, M. W., Fisher, B. M., Eldering, A., Avery, M. (2006). Ozone-CO correlations determined by the TES satellite instrument in continental outflow regions. *Geophys. Res. Lett.*, 33, L18804.
- [38] Wetter, T. (1998). *Eine Untersuchung zur Charakterisierung der Zeitlichen Variabilität der luftchemischen Bedingungen am Taunus-Observatorium: Messungen des CO und H<sub>2</sub> Mischverhältnisses im Winter 1996/7.* Johan Wolfgang Goethe-Universität, Fachbereich Geowissenschaft, Frankfurt am Main.